Check for updates

Ga^III triarylcorroles with push–pull substitutions: synthesis, electronic structure and biomedical applications†

Yingjie Niu,‡[a] Lin Wang,‡[b] Yingxin Guo,[c] Weihua Zhu, [ID][a] Rodah C. Soy,[d] Balaji Babu,[d] John Mack, [ID] *[d] Tebello Nyokong, [ID][d] Haijun Xu [ID] *[c] and Xu Liang [ID] *[a]

Two A$_2$B type H$_3$corroles and two Ga^III triarylcorroles with carbazole substitutions at 10-positions were synthesized and characterized. An analysis of structure–property relationships of the corroles has been carried out by investigating the optical spectroscopy of the dyes to trends predicted in DFT and TD-DFT calculations. Interestingly, the photodynamic therapy (PDT) and photodynamic antimicrobial chemotherapy (PACT) activity properties of the Ga^III triarylcorroles were determined against the MCF-7 breast cancer line, and *Staphyloccocus aureus* (*S. aureus*) and *Escherichia coli* (*E. coli*), respectively. The cationic **G-2Q** species exhibited the most favorable properties with an IC$_{50}$ value of 7.8 μM against MCF-7 cells, and Log reduction values of 7.78 and 3.26 against planktonic *S. aureus* and *E. coli* at 0.5 and 10 μM, respectively.

Introduction

Photodynamic therapy (PDT), one of the most attractive next generation biomedical treatment methods, is a clinically approved and non-invasive cancer treatment that facilitates the selective eradication of cancer cells through the selective accumulation of a photosensitizer dye in cancer cells. Irradiation with light of a suitable wavelength generates singlet oxygen and other reactive oxygen species (ROS).[1–4] Energy transfer from the T$_1$ state of the photosensitizer dye to ground state dioxygen forms singlet oxygen ($^1O_2$), and this causes damage to the cancer tumor. The photosensitizer dye should be highly photostable with intense absorbance in the therapeutic window (620–850 nm) and minimal dark toxicity. Selective uptake and accumulation in the cancer cells are also necessary. In a similar manner, singlet oxygen and other ROS can be generated as an anti-bacterial treatment during photodynamic antimicrobial chemotherapy (PACT) to provide an

alternative to antibiotics that are facing growing issues with resistance in the context of hospital superbugs.[5] Bacteria are classified as either Gram-(+) or Gram-(−) based on differences in the cell wall structure. The former possess a thick peptidoglycan layer and have no lipid layer, while the latter have a thin peptidoglycan layer and a lipid layer. The absence of a lipopolysaccharide layer in Gram-(+) bacteria, such as *Staphyloccocus aureus* (*S. aureus*), facilitates the uptake of neutral, cationic and anionic photosensitizer dyes. In contrast, Gram-(−) strains, such as *Escherichia coli* (*E. coli*), are resistant toward neutral and anionic photosensitizer dyes.[6] Corroles are porphyrin analogues that contain a direct pyrrole–pyrrole bond.[7–10] Their dye properties have attracted considerable interest in a wide variety of different fields,[10] including PDT[7,11–18] and PACT.[19] Due to the smaller central cavity, the corrole ligand stabilizes higher valent central ions.[20] The lower C$_{2v}$ molecular symmetry results in enhanced red region absorbance, making these dyes potentially suitable for use as photosensitizers in photodynamic therapy. Although much of the research on corroles has focused on the complexes of first-row transition metal ions, which tend to be nonfluorescent due to the presence of low-lying charge transfer states associated with the central metal, studies on non-metallic corroles became more and more popular, due to their attractive properties and low biological toxicity. The potential utility of Ga^III triarylcorroles for photodynamic therapy[21–23] and bioimaging[2,13] applications in cancer cells has previously been explored. Metallation with heavy ions, such as Ga^III, enhances the rate of intersystem crossing and the efficient generation of singlet oxygen. Axial ligands can also decrease aggregation

[a] School of Chemistry and Chemical Engineering, Jiangsu University, Zhenjiang 212013, P. R. China. E-mail: liangxu@ujs.edu.cn

[b] Affiliated Hospital of Jiangsu University, Jiangsu University, Zhenjiang 212013, P. R. China

[c] Jiangsu Co-Innovation Center of Efficient Processing and Utilization of Forest Resources, College of Chemical Engineering, Nanjing Forestry University, Nanjing 210037, P. R. China. E-mail: xuhaijun@njfu.edu.cn

[d] Institute for Nanotechnology Innovation, Department of Chemistry, Rhodes University, Makhanda 6140, South Africa. E-mail: j.mack@ru.ac.za

†Electronic supplementary information (ESI) available. See DOI: https://doi.org/10.1039/d2dt01262f

‡These two authors were contributed equally.
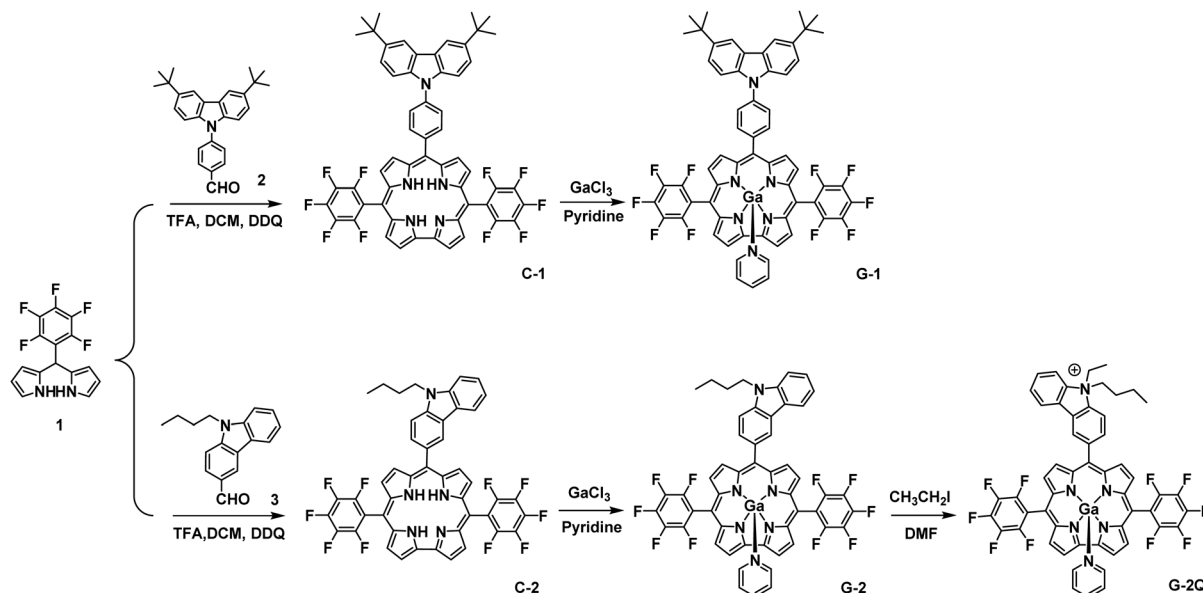
Scheme 1 Synthesis of H₃triarylcorroles **C-1** and **C-2**, Ga^III triarylcorroles **G-1** and **G-2** and a cationic species with a quaternized nitrogen, **G-2Q**.

effects caused by π–π stacking. This can facilitate enhanced cellular uptake and biodistribution. More importantly, carbazole-based organic materials have been widely employed in electronic devices due to their unique charge-transporting properties and pronounced thermal stability, while carbazole-substituted porphyrins have exhibited enhanced anti-cancer activity.[24]

There is an ongoing need to identify novel photosensitizer dyes that can be prepared with relatively easy synthetic methods that can easily be scaled up on a commercial scale. In this study, the Ga^III complexes of two asymmetric A₂B type *meso*-triarylcorroles with push–pull properties were prepared with electron-withdrawing pentafluorophenyl rings at the A₂ positions and electron-donating groups at the B position with carbazole nitrogen atoms (Scheme 1). Pentafluorophenyl-dipyrromethane was reacted with 9-(4-formylphenyl)-3,6-di-*tert*-butyl-9H-carbazole (**C-1**, **G-1**) and *N*-butyl-4-carbazole-3-carboxaldehyde (**C-2**, **G-2**), and the carbazole nitrogen atom of Ga^III triarylcorrole **G-2** was quaternized with methyl iodide to form a cationic species (**G-2Q**). The heavy atom effect of Ga^III ion in the corrole cavity enhances the rate of intersystem crossing and hence the generation of singlet oxygen,[8,25] making the **G-1** and **G-2** dyes potentially suitable for use in biomedical applications such as PDT and PACT. The axial pyridine ligand and alkyl groups on the carbazole moieties are expected to limit aggregation effects. In this study, the PDT and PACT activity properties of **G-1** and **G-2** were investigated against MCF-7 cancer cells, and *S. aureus* and *E. coli*, respectively, along with those of a cationic species **G-2Q** (Scheme 1) to enhance the suitability of the dye for use in PACT against Gram-(−) bacteria. Attempts to form a similar stable species from **G-1** proved unsuccessful. The potential utility of **G-1** and **G-2** as pH sensors due to spectral changes related to the proto-

nation properties of the carbazole nitrogen atom is also investigated in a similar manner to a recent study on an A₂B type Ga^III triarylcorrole.[26]

Experimental

General

Details of the materials and methods, and experimental details for the PDT activity, cellular uptake, lipophilicity, antimicrobial, photostability, photophysicochemical and theoretical calculation studies are provided as ESI.†

Synthesis

Pentafluorophenyldipyrromethane **1** (Scheme 1) was prepared according to literature procedures,[26] while 9-(4-formylphenyl)-3,6-di-*t*-butyl-9H-carbazole (**2**) and *N*-butyl-4-carbazole-3-carboxaldehyde (**3**) were purchased commercially from Aladdin Reagents and used without further purification. The synthetic and characterization details are provided as ESI.†

Results and discussion

Synthesis and characterization

G-1 and **G-2** were synthesized from the corresponding free base corroles (Scheme 1) and characterized by mass spectrometry (Fig. S1–S5†) and ¹H NMR spectroscopy (Fig. S6–S10†) and are reported as ESI.† Firstly, the high-resolution ESI-mass spectral data of **G-1** (Fig. S3†) revealed a strong parent peak at $m/z = 1128.2543$ (calcd for $C_{62}H_{41}F_{10}GaN_6\ [M]^+ = 1128.2483$), which indicates that the target Ga^III triarylcorrole was obtained with an axially coordinated pyridine ligand.

Similar intense parent peaks were also observed for **C-1** and **C-2** (Fig. S1 and S2†) and **G-2**. (Fig. S4†). The chemical shifts of **C-1** at 8.51–9.05 ppm can be assigned as the eight protons from pyrrole rings (Fig. S6†), and the chemical shifts at 8.18–8.35 and 7.53–7.91 ppm can be assigned as the four protons from benzo-ring and six protons from carbazole ring, respectively. Additionally, the chemical shifts of **G-1** at 8.83–9.27 ppm can be assigned as the eight protons of the pyrrole rings (Fig. S8†), and those at 8.27–8.37 and 7.63–7.96 ppm can be assigned to the four benzo ring protons and six carbazole protons, respectively. In a similar manner, the chemical shifts at 3.73 and 6.69 ppm can be assigned to the axially coordinated pyridine of **G-1**, and the chemical shifts at around 1.50 ppm can be assigned to the *tert*-butyl moiety for both **C-1** and **G-1**. **C-2** and **G-2** have similar chemical shift values to those of **C-1** and **G-1**. Finally, these compounds were also characterized by elemental analysis and FT-IR spectra (Fig. S12 and S13, see ESI†). The results confirm the satisfactory purity of the target molecules.

Electronic structure

UV-visible absorption. The UV-visible absorption spectra of **C-1** and **C-2** have similar intense B (or Soret) band absorptions at 416 nm with weaker Q-bands at 565, 613 and 644 nm (Fig. 1). These spectra are consistent with the typical absorption properties of low symmetry H_3corroles.[20,27] **G-1** and **G-2** exhibit a red-shift of the B-band absorption at 416 nm, while symmetry-split *x*- and *y*-polarized Q-bands lie at 576 and 604 nm. A comparison of the experimental data with TD-DFT calculations demonstrates that the optical spectra of **G-1** and **G-2** are dominated by Q and B electronic transitions associated with the corrole ligand (Fig. 2a and Table S1, see ESI†) and that their B position *meso*-aryl groups have a relatively minor effect as their spectra are predicted to be very similar to those calculated for the A_3 type **G-F** and **G-H** model complexes. Considering that solvent polarity has a large influence on the optical properties of molecular dyes, we analyzed the UV-visible absorption spectra of **G-1** and **G-2** in several solvents, including methanol, CH_2Cl_2, CH_3CN, THF, toluene, benzene, acetone and DMSO. The data shown in Table S1† demonstrate that solvent polarity has a large influence on the absorption properties, such as the λ_{max} values and absorption intensities.
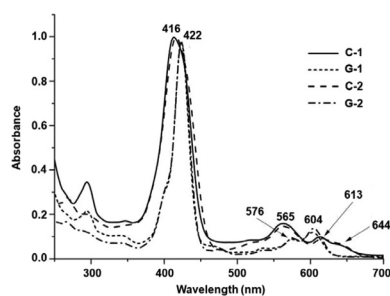
Fig. 1 UV-visible absorption spectra of **C-1**, **C-2**, **G-1** and **G-2** in CH_2Cl_2.
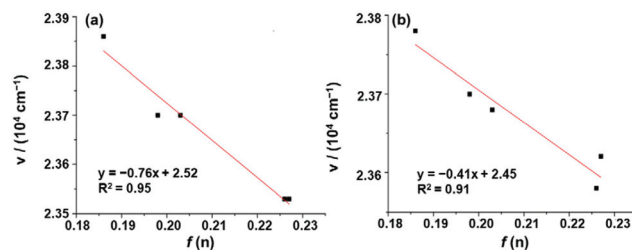
Fig. 2 Correlation of the energy in wavenumbers of the B band maxima, ν, with the Bayliss function for (a) **G-1** and (b) **G-2**.

The relationship between solvent refractive index (n), solvent permittivity (ε, if $\varepsilon < 10$, the solvent is non-polar; $\varepsilon > 10$, the solvent is polar) and the wavenumbers values for the B band maxima are summarized according to Bayliss functions with eqn (1) and (2):

$$f(n) = (n^2 - 1)/(2n^2 + 1) \quad (1)$$

$$f(n, \varepsilon) = (\varepsilon - 1)/(\varepsilon - 2) - (n^2 - 1)/(2n^2 + 1) \quad (2)$$

A strong linear correlation was observed between $f(n)$ and the energy in wavenumbers of the B band maxima (ν) for **G-1** and **G-2** in the non-polar solvent region (Fig. 2), indicating that the dispersion effect has a larger influence. On the other hand, ν and $f(n, \varepsilon)$ have no specific correlation for either dye, which is consistent with an exchange interaction between a highly polar solvent molecule and an axially coordinated pyridine molecule.

The electronic properties and optical spectroscopy of *meso*-triaarylcorroles can be conceptualized as arising from the π-MOs associated with the 15 atom 18 π-electron inner ligand perimeter that is derived from a parent $C_{15}H_{15}^{3-}$ hydrocarbon perimeter with an $M_L = 0, \pm1, \pm2, \pm3, \pm4, \pm5, \pm6, \pm7$ sequence in ascending energy terms. Since the HOMO and LUMO have M_L values of ±4 and ±5, this is analogous to Gouterman's 4-orbital model[28] for porphyrins which predicts the presence of an allowed B band based on the $\Delta M_L = \pm1$ transition at higher energy and forbidden Q-bands arising from the $\Delta M_L = \pm9$ transitions at lower energy.[20,27] To facilitate the comparison of the frontier MOs of the different complexes, Michl[29] referred to frontier π-MOs derived from the HOMO and LUMO of the parent perimeter, which have angular nodal planes that lie on the *y*-axis as **a** and **-a** MOs, while those with large MO coefficients on the *y*-axis are referred to as **s** and **-s** MOs (Fig. 2b).

TD-DFT calculations. In contrast with metalloporphyrins, corrole complexes lack four-fold symmetry. This results in a significant lifting of the degeneracy of the **-a** and **-s** MOs for symmetry reasons (Fig. 3c) and hence in a mixing of the forbidden and allowed properties of Q and B bands.[20,27,29] This results in a slight relative intensification of the Q-bands for corroles that potentially makes the dyes more suitable for use as photosensitizer dyes in biomedical applications. A marked stabilization of the frontier MOs of **G-1** and **G-2** is predicted relative to those of **G-H** due to the electron-withdrawing induc-
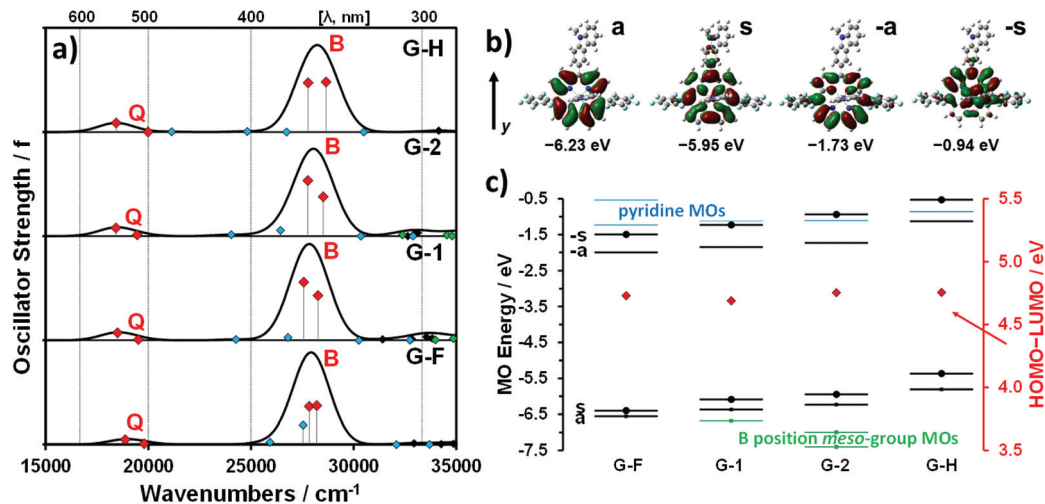
Fig. 3 (a) TD-DFT spectra for **G-F**, **G-1**, **G-2** and **G-H** at the CAM-B3LYP/SDD level of theory. The Q and B bands are highlighted with red diamonds, while blue and green diamonds are used for transitions into MOs localized on the axial pyridine ligand and out of MOs localized on the B position *meso*-aryl group, respectively. The Chemcraft software package was used to generate simulated spectra with a fixed bandwidth of 2000 cm^{-1}. (b) MO energies and angular nodal patterns of the **a**, **s**, **-a** and **-s** MOs of **G-2** at an isosurface of 0.02 a.u. (c) MO energies for **G-F**, **G-1**, **G-2** and **G-H** at the CAM-B3LYP/SDD level of theory. The **a**, **s**, **-a** and **-s** MOs are highlighted with thicker black lines, while blue and green lines are used for the MOs localized on the axial pyridine ligand and the B position *meso*-aryl group, respectively. Small black or green squares denote occupied MOs, while larger black circles highlight the **s** and **-s** MOs. Red diamonds highlight the HOMO–LUMO gap values. Details of the calculations are provided as ESI in Fig. S1,† Table S9, see ESI.†

tive effects of the *meso*-pentafluorophenyl groups at the A$_2$ positions. The presence of the electron-donating B position aryl groups results in a relative destabilization of the **s** and **-s** MOs of **G-1** and **G-2**, which have a large MO coefficient on the *meso*-carbon that is aligned with the *y*-axis (Fig. 3b and c), in comparison with the **G-F** model complex which has three electron-withdrawing *meso*-pentafluorophenyl groups due to mesomeric effects.

Fluorescence. The free base and Ga^{III}triarylcorroles emit strongly in solution (Fig. 4). In CH$_2$Cl$_2$, **C-1** and **C-2** have intense emission bands at 657 and 662 nm with the additional shoulder peak at 725 and 728 nm, respectively. On the other hand, Ga^{III}triarylcorroles have typical two-wavelength emitting properties, which can be assigned to the main Q$_{00}$ electronic transition at higher energy and a vibrational overtone on the basis of Kasha's rule.[30] The absence of mirror symmetry with the corresponding absorption spectrum (Fig. 1 and 4) provides

evidence that the higher energy band in the Q band region of the absorption spectrum can be assigned as being primarily electronic rather than vibrational in origin. The Ga^{III}triarylcorroles exhibit blue-shifted emission bands at 609, 624 nm (**G-1**) and 616, 628 (**G-2**), respectively, since the introduction of a Ga^{III} ion results in a more rigid planar structure. In order to understand the influence of organic solvents on the fluorescence properties of **G-1** and **G-2** were also measured in MeOH, CH$_2$Cl$_2$, CH$_3$CN, THF and toluene (Fig. 5 and Table S2, see ESI†). In lower polarity solvents, **G-1** and **G-2** exhibit red-shifted emission band wavelengths, but higher fluorescence quantum yield (Φ_F) values. **G-2** exhibits a redshift of the emission bands compared with those of **G-1**. For example, **G-1** has two emission bands at 610 and 662 nm with a Φ_F value of 12.60% in THF, but **G-1** exhibits emission bands at 610 and 669 nm with a Φ_F value of 10.80%. **G-1** and **G-2** have higher fluorescence quantum yield and radiation transition rate constants than **C-1** and **C-2** (Table S3, see ESI†), since the penta-coordination of Ga^{III}triarylcorroles with axial

Fig. 4 The steady-state fluorescence spectra of **C-1**, **C-2**, **G-1** and **G-2** in CH$_2$Cl$_2$.
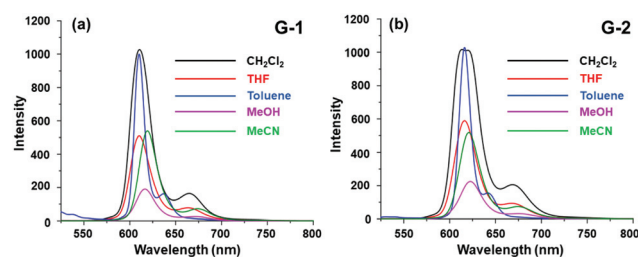
Fig. 5 Fluorescence spectra of **G-1** (a) and **G-2** (b) in various solvents.

pyridine ligands enhances the rigidity of the molecular plane. The fluorescence lifetime (τ_F) values of **G-1** and **G-2** are significantly shorter than those of **C-1** and **C-2** due to the heavy atom effect of gallium, which promotes intersystem crossing to the triplet manifold. According to Franck–Condon law, the increase of non-radiative decay also shortens the fluorescence lifetime of compounds. A series of pH-dependent spectroscopic experiments were carried out in a mixed solvent of H_2O and CH_3CN (v/v = 1 : 9, $C = 1.0 \times 10^{-5}$ M), and the pH values were controlled by the addition of trifluoracetic acid (TFA) for protonation and NH_4OH for deprotonation of the N atom of the carbazole unit group. It should be noted that the solution color and spectral properties resulted in few to no changes in any of the measurements. In Fig. 6a and c, the B-band intensities of **G-1** and **G-2** were significantly decreased when lower pH values were applied, and new absorptions were slightly increased at *ca.* 480 nm. Compared with B band absorptions, the changes in Q-band regions became much weaker upon decreasing the pH values. In contrast, the fluorescence intensities of **G-1** (Fig. 6b) and **G-2** (Fig. 6d) gradually decreased under acidic conditions as the pH was decreased from 6.51 to 0.97, and no obvious spectral shifts were observed. This observation suggests that a new species was formed due to the protonation of the N atom of the carbazole moieties, which results in a quenching of a photoinduced electron transfer (PET) process. The quenched PET process may also decrease the molar absorption coefficients of these Ga^{III}corroles. The data shown here hence provide a plausible mechanism for the observed decreases in absorbance and fluorescence intensity. In contrast, as shown in Fig. S11 in the ESI,† when the pH was increased from 7.50 to 13.4, the fluorescence intensity of Ga^{III}triarylcorroles **G-1** and **G-2** exhibit little to no change in both the UV-vis absorption and fluorescence spectra. This can be attributed to the carbazole N atom being uniquely sensitive

to a low pH environment and unreactive at high pH values. The electron-rich carbazole-substituents can quench the fluorescence of the Ga^{III}triarylcorroles due to the PET process in acidic media. The dependence of the fluorescence intensity of **G-1** and **G-2** on pH is typical of an "on–off" mechanism (Scheme 2). The significant changes in the absorption and fluorescence properties of **G-1** and **G-2** imply that these Ga^{III}triarylcorroles could be used as highly sensitive probes for detecting pH changes under acidic conditions. In principle, the Ga^{III}triarylcorroles in this study can serve as both electron donors and acceptors upon photoexcitation. Photoinduced electron transfer can occur from the excited Ga^{III}triarylcorrole moiety to the LUMO of the carbazole moiety (donor-excited PET; d-PET).

Photodynamic activities

General. The wavelengths of the major spectral bands of **G-1**, **G-2** and **G-2Q** vary to only a minor extent in DMSO in the UV-visible absorption and fluorescence emission spectra (Table S4, see ESI†), since the A$_2$B type *meso*-triarylcorrole structures of **G-1** and **G-2** are very similar. The Φ_Δ values for **G-1**, **G-2** and **G-2Q** in DMSO are moderately high, ranging from 0.64–0.67 (Table S4,† see ESI†) while the Φ_F values are relatively low, ranging from 0.062–0.073 since Ga^{III} is a relatively heavy atom that enhances the rate of intersystem crossing to the T$_1$ state. The triplet state lifetime (τ_T) value of **G-2Q** of 42.4 μs is significantly shorter than those of **G-1** and **G-2** (255 and 193 μs, respectively) when the DMSO solutions are purged
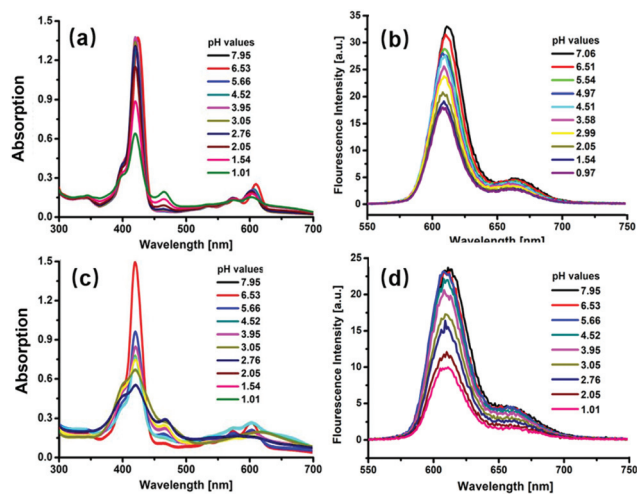
Fig. 6 UV-vis absorption (a and c) and fluorescence emission (b and d) spectra of Ga^{III}triarylcorroles **G-1** (a and b) and **G-2** (c and d) a mixed solvent of H_2O and CH_3CN (1 : 9) with an excitation wavelength of 500 nm under various pH conditions.
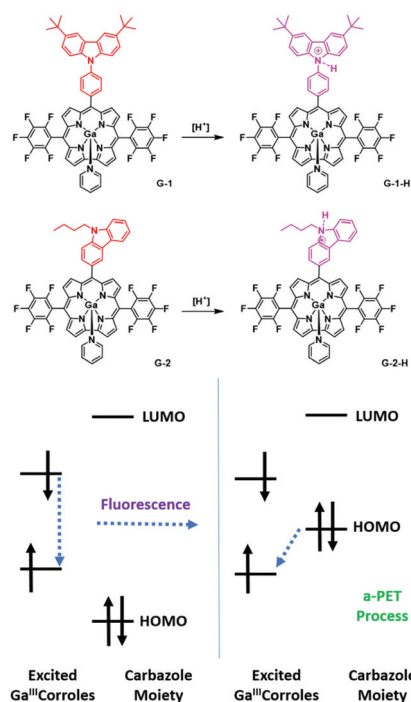
Scheme 2 Proposed mechanism of the photoinduced electron transfer between the Ga^{III}triarylcorrole moiety and carbazole unit of **G-1** and **G-2** in protonated quinolinium, neutral, and deprotonated quinolinate states, respectively.

with nitrogen gas (Table S4, see ESI†), but is more comparable in the presence of oxygen when this is not done. The τ_F values of all three dyes lie in the 1.54–1.74 µs range (Table S4, see ESI†), which is shorter than the values of 2.62–3.08 µs that have been reported for a series of A_3 type Ga^{III}triarylcorroles.[21] The properties of **G-1** and **G-2** make them potentially suitable for use in biomedical applications such as PDT and PACT.

Lipophilicity studies. The lipophilicities of **G-1**, **G-2** and **G-2Q** determined by the shake flask method are provided in Table S5.† The Log $P_{o/w}$ values of **G-2** and **G-2Q** are lower than that of **G-1**, so **G-2** is less lipophilic. Ideally, a drug should have a log P value of between 0–5 to achieve the proper balance between aqueous solubility and cell permeability, so these results suggest that **G-1**, **G-2** and **G-2Q** are potentially promising for use as photosensitizer dyes.

Photostability studies. Photodegradation of photosensitizer dyes can occur during PDT and PACT related experiments due to the generation of $^1O_2$, resulting in side products and can decrease PDT efficacy.[31,32] Ideally, the photosensitizer dye should remain stable under illumination during the PDT activity experiments.[1,2,31,32] The photostabilities of **G-1**, **G-2** and **G-2Q** are compared in Table S6, see ESI.† In each case, the degradation under the same conditions used for the PDT activity experiments were <10%.

Cellular uptake. Cellular uptake studies were performed with MCF-7 cells at 10 µg mL^{-1} after incubation with **G-1**, **G-2** and **G-2Q** for 24 h (Fig. 7). **G-2Q** exhibits higher fluorescence intensity. Since all three Ga^{III} complexes have similar fluorescence quantum yields (Table S1, see ESI†), this provides evidence that uptake of **G-2Q** is significantly enhanced.

Cytotoxicity studies. The *in vitro* dark cytotoxicity properties and PDT activities of **G-1**, **G-2** and **G-2Q** against the MCF-7 cell line were investigated over a dye concentration range of 0.7–50 µM in the dark and under illumination with a Thorlabs M595L3 LED. Table S2† summarizes the dark cytotoxicity properties and the IC$_{50}$ and phototoxicity index (PI) values obtained, while Fig. 9 provides the cytotoxicity plots. Low dark cytotoxicity is desirable, since this prevents cytocidal activity from occurring against both healthy and cancerous cells in the absence of light.[3,4] **G-1**, **G-2** and **G-2Q** were found to have dark toxicity IC$_{50}$ values >50 µM (Fig. 8). This demon-
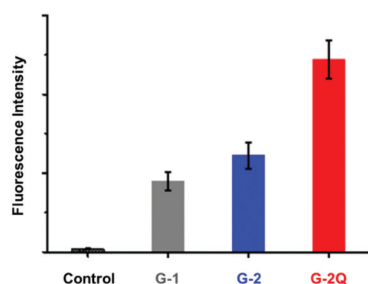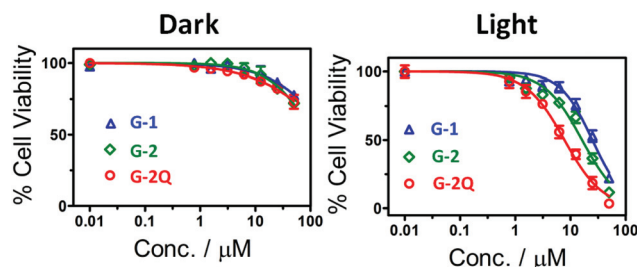
Fig. 8 Percentage cell viabilities of MCF-7 cancer cells after 24 h incubation with a gradient concentration of the drugs in the dark and under illumination for 20 min at 595 nm with a Thorlabs M595L3 LED (cells quantification using the MTT assay).

strates that they are relatively non-toxic in this context. The PDT activities of **G-1**, **G-2** and **G-2Q** were determined over 20 min of illumination at a fixed light dose of 300 J cm^{-2}, Fig. 8. As would be anticipated based on its higher cellular uptake, **G-2Q** exhibited a higher PDT activity than **G-1** and **G-2** (Table S8, see ESI†) with a relatively low IC$_{50}$ value of 7.8 µM and a phototoxicity index value of >6.45 (Table S7, see ESI†).

Photodynamic antimicrobial activities of G-1, G-2 and G-2Q. Photodynamic antimicrobial activity studies were carried out at 595 nm with a Thorlabs M595L3 LED (250 mW cm^{-2}) for **G-1**, **G-2** and **G-2Q** against both planktonic and biofilms cells of *S. aureus* and *E. coli* that were selected to provide typical examples of Gram-(+) and Gram-(−) bacteria, respectively. For planktonic cells, only the direct method was considered for the estimation of viable cells using the viable colony count method by counting viable colonies formed on the agar plates with a bacteria counter. In contrast, both direct and indirect methods were used to quantify the biofilm cells. Crystal violet assay was used to quantify biofilm cells indirectly by staining the biofilms and determining the absorbance value at 590 nm on a Synergy 2 multi-diode microplate reader (BioTek). **G-2Q** exhibits significantly higher photodynamic antimicrobial activity against *S. aureus* than **G-2** and **G-1** (Fig. 9 and Table S7, see ESI†), probably due to the cationic nature of this species. In the context of *E. coli*, all three dyes exhibit significant photodynamic antimicrobial activity at 10 µM, with only **G-2Q** exhibiting a Log reduction of >3.0, which is the value required for a molecular dye to be viewed as an efficient antimicrobial agent in this context by the Food & Drug Administration of the USA.[33] The relatively favorable results obtained for **G-1** and **G-2** dyes in this context may be due to the push–pull properties associated with the A_2B *meso*-substitution pattern. In a similar manner, the PACT activities were also determined against biofilms cells of *S. aureus* and *E. coli* in the dark and light upon treatment at gradient concentrations of 15, 30, 60, 120 and 240 µM. **G-1**, **G-2**, and **G-2Q** exhibited moderately high photoinactivation activity towards biofilms of *S. aureus* at relatively low dye concentrations, with significant photoinactivation activity also observed toward *E. coli* (Fig. 10 and Table S8, see ESI†).

Fig. 7 Fluorescence intensities plots of the cells against concentration after incubation for 24 h with 10 µM of the samples; fluorescence measured at 640 nm.
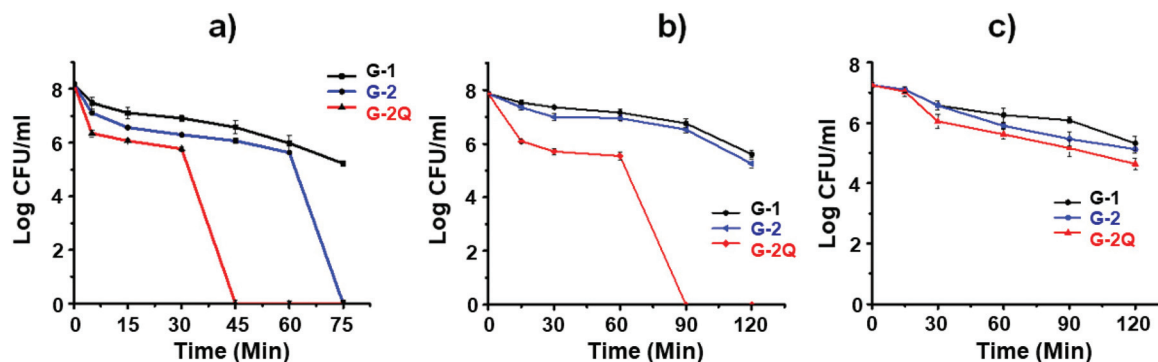
Fig. 9 Plots of Log CFU mL^{-1} of planktonic cells of (a) and (b) *S. aureus*, and (c) *E. coli* upon treatment with (a) 0.5 µM, (b) 2.5 µM and (c) 10 µM of **G-1**, **G-2** and **G-2Q** after irradiation for (a) 75 min, (b) and (c) for 120 min at 595 nm with a Thorlabs M595L3 LED (250 mW cm^{-2}).
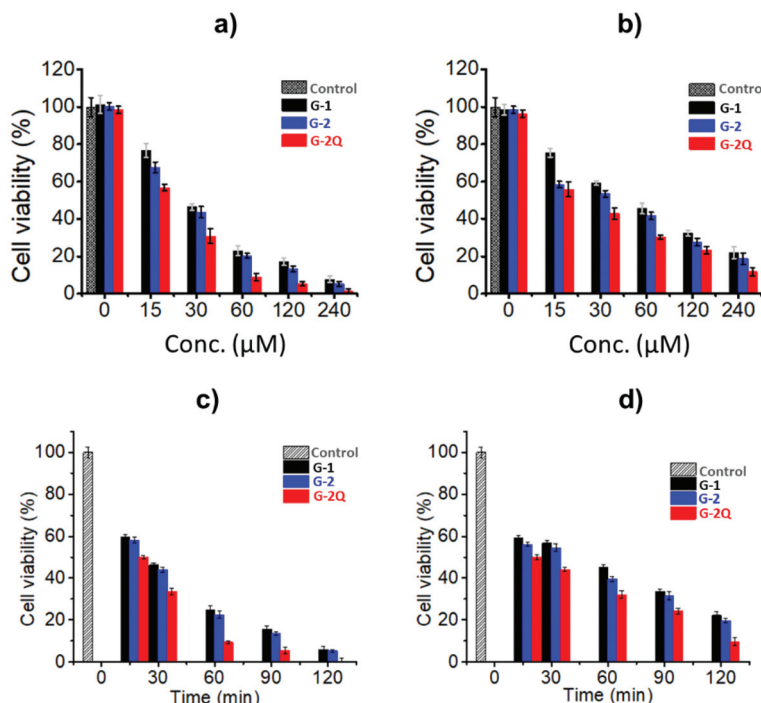
Fig. 10 Percentage cell viabilities of biofilm cells of (a) *S. aureus*, and (b) *E. coli* upon treatment with gradient concentrations of **G-1**, **G-2** and **G-2Q** after 30 min irradiation at 595 nm with a Thorlabs M595L3 LED (250 mW cm^{-2}) with quantification by crystal violet stain. Percentage cell viabilities of biofilm cells of, (c) *S. Aureus*, and (d) *E. Coli*, upon treatment with, (c) 30 µM, and (d) 60 µM, of **G-1**, **G-2** and **G-2Q** after 120 min irradiation at 595 nm with a Thorlabs M595L3 LED (250 mW cm^{-2}).

Conclusions

In summary, two novel Ga^{III}triarylcorroles with push–pull properties have been successfully synthesized with electron-withdrawing pentafluorophenyl rings at the A$_2$ positions and electron-donating groups at the B position that contain carbazole moieties. The carbazole nitrogen atom of the *meso*-3-*N*-butyl-carbazole group of **G-2** was quaternized with methyl iodide to form a cationic species. **G-1**, **G-2** and **G-2Q** were found to have moderately high singlet oxygen quantum yields in the 0.64–0.67 range in DMSO due to the heavy atom effect of the

central ion. The PDT and photodynamic PACT activity properties were determined at 595 nm against the MCF-7 breast cancer line, and *S. aureus* and *E. coli*, respectively, with a Thorlabs M595L3 LED. The PACT studies were carried out against both planktonic and biofilm bacteria. In each case, the cationic **G-2Q** species exhibited the most favorable properties with an IC$_{50}$ value of 7.8 µM against MCF-7 cells, and Log reduction values of 7.78 and 3.26 against planktonic *S. aureus* and *E. coli* at 0.5 and 10 µM, respectively. **G-1** and **G-2** were found to be potentially suitable for use as pH sensors. Spectral changes are observed related to the protonation pro-

perties of the carbazole nitrogen atom on the B position *meso*-aryl group.

Conflicts of interest

There are no conflicts to declare.

Acknowledgements

Notes and references

1 B. W. Henderson and T. J. Dougherty, How does photodynamic therapy work?, *Photochem. Photobiol.*, 1992, **55**, 145–157, DOI: **10.1111/j.1751-1097.1992.tb04222.x**.

2 R. R. Allison and K. Moghissi, Photodynamic therapy (PDT): PDT mechanisms, *Clin. Endosc.*, 2013, **46**, 24–29, DOI: **10.5946/ce.2013.46.1.24**.

3 H. Abrahamse and M. R. Hamblin, New photosensitizers for photodynamic therapy, *Biochem. J.*, 2016, **473**, 347–364, DOI: **10.1042/BJ20150942**.

4 A. B. Ormond and H. S. Freeman, Dye sensitizers for photodynamic therapy, *Materials*, 2013, **6**, 817–840, DOI: **10.3390/ma6030817**.

5 M. Wainwright, Photodynamic antimicrobial chemotherapy (PACT), *J. Antimicrob. Chemother.*, 1998, **42**, 13–28, DOI: **10.1093/jac/42.1.13**.

6 S. George, M. R. Hamblin and A. Kishen, Uptake pathways of anionic and cationic photosensitizers into bacteria, *Photochem. Photobiol. Sci.*, 2009, **8**, 788–795, DOI: **10.1039/B809624D**.

7 I. Aviv and Z. Gross, Corrole-based applications, *Chem. Commun.*, 2007, 1987–1999, DOI: **10.1039/B618482K**.

8 V. K. Sharma, M. Stark, N. Fridman, Y. G. Assaraf and Z. Gross, Doubly Stimulated Corrole for Organelle-Selective Antitumor Cytotoxicity, *J. Med. Chem.*, 2022, **65**, 6100–6115, DOI: **10.1021/acs.jmedchem.1c02085**.

9 R. Orłowski, D. Gryko and D. T. Gryko, Synthesis of Corroles and Their Heteroanalogs, *Chem. Rev.*, 2017, **117**, 3102–3137, DOI: **10.1021/acs.chemrev.6b00434**.

10 C. Di Natale, C. P. Gros and R. Paolesse, Corroles at work: a small macrocycle for great applications, *Chem. Soc. Rev.*, 2022, **51**, 1277–1335, DOI: **10.1039/D1CS00662B**.

11 J. Oppenheim, M. H. B. Gray, A. J. Di Bilio, B. J. Brennan, L. M. Henling, P. Lim, M. Soll, J. Termini, S. C. Virgil, Z. Gross and H. B. Gray, Structures and Spectroscopic Properties of Metallocorrole Nanoparticles, *Inorg. Chem.*, 2019, **58**, 10287–10294, DOI: **10.1021/acs.inorgchem.9b01441**.

12 J. Y. Hwang, J. Lubow, D. Chu, J. Ma, H. Agadjanian, J. Sims, H. B. Gray, Z. Gross, D. L. Farkas and L. K. Medina-Kauwe, A mechanistic study of tumor-targeted corrole toxicity, *Mol. Pharm.*, 2011, **8**, 2233–2243, DOI: **10.1021/mp200094w**.

13 R. D. Teo, J. Y. Hwang, J. Termini, Z. Gross and H. B. Gray, Fighting cancer with corroles, *Chem. Rev.*, 2016, 2711–2729, DOI: **10.1021/acs.chemrev.6b00400**.

14 Z. Zhang, H. J. Yu, H. Huang, H. H. Wang, S. Wu, H. Y. Liu and H. T. Zhang, The photodynamic activity and toxicity evaluation of 5,10,15-tris(ethoxylcarbonyl) corrole phosphorus(V) in vivo and in vitro, *Eur. J. Med. Chem.*, 2019, **163**, 779–786, DOI: **10.1016/j.ejmech.2018.12.031**.

15 M. Pribisko, J. Palmer, R. H. Grubbs, H. B. Gray, J. Termini and P. Lim, Cellular uptake and anti-cancer activity of carboxylated gallium corroles, *Proc. Natl. Acad. Sci. U. S. A.*, 2016, **113**, E2258–E2266, DOI: **10.1073/pnas.1517402113**.

16 B. Babu, E. Prinsloo, J. Mack and T. Nyokong, Synthesis, characterization and photodynamic activity of Sn(IV) triarylcorroles with red-shifted Q bands, *New J. Chem.*, 2019, **43**, 18805–18812, DOI: **10.1039/C9NJ03391B**.

17 S. Dingiswayo, B. Babu, E. Prinsloo, J. Mack and T. Nyokong, A comparative study of the photophysicochemical and photodynamic activity properties of meso-4-methylthiophenyl functionalized Sn(IV) tetraarylporphyrins and triarylcorroles, *J. Porphyrins Phthalocyanines*, 2020, **24**, 1138–1145, DOI: **10.1142/S1088424620500273**.

18 B. Fu, Y. Niu, X. Yu, X. Fang, J. Mack, S. Dingiswayo, T. Nyokong, X. Liang and H. Xu, Borneol-triarylcorrole hybrids with chiral-optical response and anticancer behaviours, *Dyes Pigm.*, 2021, **195**, 109699, DOI: **10.1016/j.dyepig.2021.109699**.

19 T. A. F. Cardote, J. F. B. Barata, C. Amador, E. Alves, M. G. P. M. S. Neves, J. A. S. Cavaleiro, Â. Cunha, A. Almeida and M. A. F. Faustino, Evaluation of meso-substituted cationic corroles as potential antibacterial agents, *An. Acad. Bras. Cienc.*, 2018, **90**, 1175–1185, DOI: **10.1590/0001-3765201820170824**.

20 J. Mack, Expanded, Contracted, and Isomeric Porphyrins: Theoretical Aspects, *Chem. Rev.*, 2017, **117**, 3444–3478, DOI: **10.1021/acs.chemrev.6b00568**.

21 R. C. Soy, B. Babu, J. Mack and T. Nyokong, The photodynamic activities of the gold nanoparticle conjugates of

phosphorus(V) and gallium(III) A_3 meso-triarylcorroles, *Dyes Pigm.*, 2021, **194**, 109631, DOI: **10.1016/j.dyepig.2021.109631**.

22 X. Jiang, R. X. Liu, H. Y. Liu and C. K. Chang, Corrole-based photodynamic antitumor therapy, *J. Chin. Chem. Soc.*, 2019, **66**, 1090–1099, DOI: **10.1002/jccs.201900176**.

23 B. Brizet, N. Desbois, A. Bonnot, A. Langlois, A. Dubois, J. Barbe, C. P. Gros, C. Goze, F. Denat and P. D. Harvey, Slow and Fast Singlet Energy Transfers in BODIPY-gallium(III)corrole Dyads Linked by Flexible Chains, *Inorg. Chem.*, 2014, **53**, 3392–3403, DOI: **10.1021/ic402798f**.

24 B. Fu, X. Y. Dong, X. X. Yu, Z. Zhang, L. Sun, W. H. Zhu, X. Liang and H. J. Xu, Meso-borneol- and meso-carbazole-substituted porphyrins: multifunctional chromophores with tunable electronic structures and antitumor activities, *New J. Chem.*, 2021, **45**, 2141–2146, DOI: **10.1039/D0NJ02954H**.

25 A. Mahammed and Z. Gross, Corroles as triplet photosensitizers, *Coord. Chem. Rev.*, 2019, **379**, 121–132, DOI: **10.1016/j.ccr.2017.08.028**.

26 F. Cai, F. Xia, Y. Guo, W. Zhu, B. Fu, X. Liang, S. Wang, Z. Cai and H. Xu, "Off–on–off" type of selectively pH-sensing 8-hydroxyquinoline-substituted gallium(III) corrole, *New J. Chem.*, 2019, **43**, 18012–18017, DOI: **10.1039/C9NJ04544A**.

27 X. Liang, J. Mack, L. M. Zheng, Z. Shen and N. Kobayashi, Phosphorus(V)-corrole: Synthesis, spectroscopic properties, theoretical calculations, and potential utility for in vivo applications in living cells, *Inorg. Chem.*, 2014, **53**, 2797–2802, DOI: **10.1021/ic402347w**.

28 M. Gouterman, *The Porphyrins, Vol III, Part A*, ed. D. Dolphin, Academic Press, New York, 1978, pp. 1–165.

29 J. Michl, Magnetic circular dichroism of cyclic π-electron systems. 1. Algebraic solution of the perimeter model for the A and B terms of high-symmetry systems with a (4N+2)-electron [n] annulene perimeter, *J. Am. Chem. Soc.*, 1978, **100**, 6801–6811, DOI: **10.1021/ja00490a002**.

30 M. Kasha, Characterization of electronic transitions in complex molecules, *Discuss. Faraday Soc.*, 1950, **9**, 14–19, DOI: **10.1039/DF9500900014**.

31 B. C. Wilson and M. S. Patterson, The physics, biophysics and technology of photodynamic therapy, *Phys. Med. Biol.*, 2008, **53**, R61, DOI: **10.1088/0031-9155/53/9/R01**.

32 S. Kwiatkowski, B. Knap, D. Przystupski, J. Saczko, E. Kędzierska, K. Knap-Czop, J. Kotlińska, O. Michel, K. Kotowski and J. Kulbacka, Photodynamic therapy-mechanisms, photosensitizers and combinations, *Biomed. Pharmacother.*, 2018, **106**, 1098–1107, DOI: **10.1016/j.biopha.2018.07.049**.

33 E. Alves, M. A. F. Faustino, M. G. P. M. S. Neves, Â. Cunha, J. Tome and A. Almeida, An insight on bacterial cellular targets of photodynamic inactivation, *Future Med. Chem.*, 2014, **6**, 141–164, DOI: **10.4155/fmc.13.211**.